REGULAR ARTICLES

Twist singularities for symplectic maps

H. R. Dullin[a)]
Department of Mathematical Sciences, Loughborough University, Loughborough LE11 3TU, United Kingdom

J. D. Meiss[b)]
Department of Applied Mathematics, University of Colorado, Boulder, Colorado 80309-0526

(Received 24 June 2002; accepted 24 October 2002; published 7 January 2003)

Near a nonresonant, elliptic fixed point, a symplectic map can be transformed into Birkhoff normal form. In these coordinates, the dynamics is represented entirely by the Lagrangian ''frequency map'' that gives the rotation number as a function of the action. The twist matrix, given by the Jacobian of the rotation number, describes the anharmonicity in the system. When the twist is singular the frequency map need not be locally one-to-one. Here we investigate the occurrence of fold and cusp singularities in the frequency map. We show that folds necessarily occur near third order resonances. We illustrate the results by numerical computations of frequency maps for a quadratic, symplectic map. © *2003 American Institute of Physics.* [DOI: 10.1063/1.1529450]

The dynamics in the neighborhood of a linearly stable periodic orbit of a Hamiltonian flow or fixed point of a symplectic map can be elucidated by consideration of their Birkhoff normal forms. The normal form has action variables, J, which are formal invariants when the rotation vector, ω, of the elliptic orbit is nonresonant. The conjugate angle variables θ rotate with a frequency vector $2\pi\Omega(J)$ that depends upon the action. When $\partial\Omega/\partial J$ is a nondegenerate matrix, the system has twist. For such systems the map from actions to frequencies is locally smooth and one-to-one; this is a requirement for the application of KAM theory which implies that sufficiently incommensurate tori persist in the full dynamics. Our goal in this article is to study the simplest degeneracies of the twist, the fold and cusp singularities. The fold has been extensively studied elsewhere for the case of area-preserving maps. Here we extend these results to higher-dimensional symplectic maps.

I. INTRODUCTION

For a symplectic map with an elliptic fixed point, the Birkhoff normal form can be written in terms of angle $\theta \in \mathbb{T}^d$ and action $J \in \mathbb{R}^d$ coordinates as

$$\theta' = \theta + 2\pi\Omega(J), \qquad J' = J. \tag{1}$$

Here $\Omega(J)$ is the rotation vector as a function of the action, and the rotation vector at the elliptic fixed point is denoted $\omega = \Omega(0)$. The fixed point is said to be nonresonant when the equation $m \cdot \omega = n$ has no solutions for $m \in \mathbb{Z}^d$ and $n \in \mathbb{Z}$. The map is symplectic when $d\theta' \wedge dJ' = d\theta \wedge dJ$, which requires that Ω be the gradient of a scalar function, $\Omega = DS(J)$. The ''twist'' of this map is defined to be the $d \times d$ dimensional matrix $\tau(J) = D\Omega(J) = D^2S$. It represents the anharmonicity of the system.

If the twist at $J=0$ is nonsingular and there are no low-order resonances, then Moser's twist theorem implies that the elliptic fixed point is a limit point of a family of invariant tori.[1,2] For the area-preserving case, this implies that the fixed point is stable. Though $\det(\tau(0))=0$ seems special, it occurs with codimension-one in the neighborhood of a tripling bifurcation of an elliptic fixed point.[3,4] That is, if variation of a parameter causes the frequency at the elliptic fixed point to cross $\frac{1}{3}$, the twist at the elliptic fixed point will generically cross zero for a nearby parameter value. Consequences of this were observed in Refs. 5–7.

Vanishing of the twist for the two-dimensional case leads to a number of phenomena, including instability,[4,8,9] reconnection bifurcations between unstable and stable manifolds of periodic orbits,[10,11] orbits that can chaotically drift among multiple island chains with the same frequency,[12] exotic ''meandering'' invariant circles,[13] and unusual renormalization structure for critical twistless invariant circles.[14–16] The structures that arise depend upon the number of vanishing derivatives of S—if j derivatives vanish, then j island chains with the same frequency can arise nearby in parameter space.[17]

Here we begin an investigation of the twist singularities that occur in the neighborhood of an elliptic fixed point of four-dimensional, symplectic maps. We start by studying the form of typical singularities in the frequency map defined by $\Omega(J)$. These singularities have been classified by Thom[18] and Arnold.[19] The stable singularities for $d=2$ are the fold and cusp.

We then study a polynomial map in the neighborhood of

[a)]Electronic mail: h.r.dullin@lboro.ac.uk
[b)]Electronic mail: james.meiss@colorado.edu

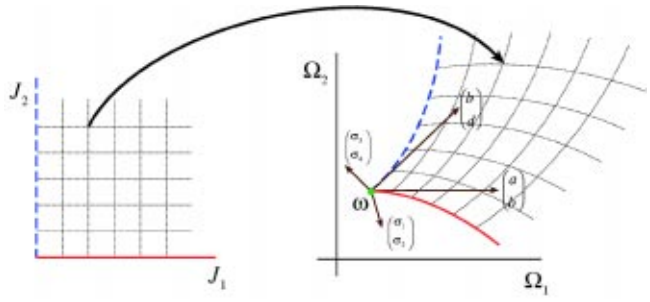

FIG. 1. (Color online) Sketch of the frequency map for $d=2$. The positive quadrant in action space is mapped to a cone in frequency space. Throughout this article the solid curves denote the J_1 axis or its image and the dashed curves the J_2 axis or its image. The vectors label the columns of τ_0 as τ_{ij} and the four entries in τ_1 as σ_i, see (6).

an elliptic fixed point. If we assume there are no low-order resonances, the map can be transformed to Birkhoff form to some finite order in a power series expansion in the actions. We compute the twist and show that it generally vanishes near several resonances. We compare the calculations of the twist with numerical calculations of the frequency map based on Laskar's algorithm[20,21] to observe the folds and cusps. Finally we use the technique of Meiss[22] to estimate the volume of the elliptic region in the neighborhood of the fixed point.

II. VANISHING TWIST

Since the frequency map is generated by S through $\Omega(J)=DS$, this map is an example of a "Lagrangian map." Recall that a d-dimensional submanifold of a symplectic manifold is Lagrangian if the symplectic form vanishes identically for any pair of tangent vectors to the submanifold. The submanifold $L=\{(\theta,J):\theta=0\}$ is Lagrangian, and its image under the Birkhoff normal form (1), $f(L)=\{(\theta,J):\theta=DS(J)\}$, is therefore also Lagrangian. Since this Lagrangian manifold is a graph over J, we can trivially project out the J direction, defining

$$J\overset{\Omega}{\mapsto}DS(J)=\omega+\tau_0 J+\frac{1}{2}J^t\tau_1 J+\cdots$$

to be the frequency map, Ω. The twist is defined to be the Jacobian of the frequency map

$$\tau(J)=D\Omega(J)=D^2S(J)=\tau_0+\tau_1 J+\cdots,$$

where τ_1 is a one-form valued matrix.

Since $J_i\geqslant 0$, the domain of the frequency map is the positive orthant in J, so that its image is a cone in Ω with vertex at ω (see Fig. 1). (Most of the figures in this article are available in color in the online version.) If the twist is nonsingular at J, then the frequency map is a diffeomorphism near J. Here we discuss the form of the singularities in the frequency map that are created as $\det\tau$ goes through zero, i.e., of the critical points of Lagrangian maps.

A. Singularities of maps

Here we briefly recall a few facts about the singularities of smooth maps.[23] A map $f:\mathbb{R}^m\to\mathbb{R}^n$ has a critical point at x if its Jacobian, $Df(x)$, has less than maximal rank, i.e., if $\operatorname{rank}(Df)<\min(m,n)$. The image, $f(x)$, of a critical point is a critical value. A map is said to be (C^k) stable at x if every map that is sufficiently close to f (in the sense that the first k derivatives are close) is locally diffeomorphic to f. The equivalence class of maps that are locally diffeomorphic to f is the "germ" of f. If the dimension is low enough, the germ can be represented by a fixed polynomial map; more generally "moduli," which are either parameters or arbitrary functions, are needed to represent the germ. The equivalence class of maps represented by the germ in the neighborhood of a critical point is called a "singularity."

For example, when $m=n=2$, there are only two stable singular germs; both correspond to singularities for which $\operatorname{rank}(Df)=1$. These are the "fold," represented by $f(x)=(x_1^2,x_2)$, and the "cusp," represented by $f(x)=(x_1^3+x_1x_2,x_2)$. The case for which the rank of Df is 0 is not stable in two dimensions. Since the fold and cusp are stable, every nearby map has nearby critical points of the same form.

B. Singularities of Lagrangian maps

A Lagrangian map is defined by the projection of a Lagrangian manifold onto a Lagrangian plane. For example, in geometrical optics the Lagrangian manifold corresponds to a wave front together with its unit normals, the velocity vectors, and the projection is to physical space. Correspondingly, the set of critical values of a Lagrangian map is called a "caustic." A Lagrangian manifold can be represented by a single, generating function;[24] if, as in our case, the Lagrangian manifold is a graph over the action space, $(\theta,J)=(DS(J),J)$, the generating function is $S(J)$. The Lagrangian map is the projection of the manifold onto the action space, i.e., $\Omega:\mathbb{R}^d\to\mathbb{R}^d$ defined by $J\mapsto DS(J)$. The map has a critical point at J if $\tau=D^2S(J)$ is singular.

The standard theory of the singularities of Lagrangian maps has been formalized by Thom and generalized by Arnold.[23] When $d=1$ there is only one stable singularity, the "fold." For $d=2$ the "cusp" singularity is also stable. For $d=3$, three new singularities are stable, the "swallowtail" and two forms of point singularities (pyramids and purses).

The fold singularity is denoted A_2. When $d=2$, a Lagrangian map with a fold is locally equivalent to the map generated by

$$S(J)=J_1^2+J_2^3. \tag{2}$$

The critical set, determined by $0=\det(D^2S)=12J_2$, is the horizontal axis. The caustic is $\Omega_c=\Omega(J_1,0)$, which is the axis $\Omega_2=0$. The action of the map is to fold the J-plane into the upper half Ω-plane.

There are two cusp singularities, denoted A_3^ϵ, where $\epsilon=\pm$. For $d=2$, the germ of these is represented by the generating function

$$S(J)=(J_1+J_2^2)^2+\epsilon J_2^4. \tag{3}$$

Here the critical set is the parabola $J_1=-(1+3\epsilon)J_2^2$, and the caustic is the semi-cubical parabola, or cusp:

$$\Omega_c = -2\epsilon \begin{pmatrix} 3J_2^2 \\ 4J_2^3 \end{pmatrix}.$$

In the exterior of the cusp, the map is one-to-one, while in the interior it is three-to-one.

Generally the set of critical points, $\det \tau = 0$, is a smooth codimension-one submanifold in J-space, i.e., a curve when $d=2$. The caustic is locally smooth whenever the image of the tangent vector to the critical set is nonzero. This tangent, v, is determined by $(D \det \tau)^T v = 0$, and its image τv is nonzero if v is not in the kernel of τ. In terms of the generating function, this condition reduces to the equation

$$\delta = S_{11}(3S_{12}S_{122} - S_{11}S_{222}) - S_{12}(3S_{12}S_{112} - S_{22}S_{111}) \neq 0, \quad (4)$$

on the curve $S_{11}S_{22} = S_{12}^2$; the subscripts on S indicate partial derivatives. When $\delta \neq 0$, the singularity is locally a fold, and when $\delta = 0$, the image is a cusp point whenever the image of the unit tangent vector is not continuous. This is generic, since it happens whenever at least one of the components of τv reverses sign upon crossing the zero.

C. Twistless bifurcations

Since the Birkhoff normal form is computed as a power series about $J=0$, and the physical domain corresponds to $J_i \geqslant 0$, we now consider singularities that occur at the origin for a map whose domain is the positive orthant. The behavior of the frequency map at the origin is determined by the rank of $\tau_0 = D^2 S(0)$. When this is less than d, the image collapses to a subspace of dimension $\mathrm{rank}(\tau_0)$. Generally, if a parameter is varied so that τ_0 goes through rank $d-1$, the orientation of the image is reversed. If we keep nonlinear terms in J, this generally corresponds to the passage of a fold caustic through $\omega = \Omega(0)$. Since the passage of $\det \tau_0$ through zero results in qualitative changes in the dynamics, we call it a "twistless bifurcation."

The critical points in the neighborhood of $J=0$ can be studied by expanding S in a series in the actions. For $d=2$, this series begins

$$S(J) = \omega \cdot J + \tfrac{1}{2} a J_1^2 + b J_1 J_2 + \tfrac{1}{2} d J_2^2 + \tfrac{1}{6}(\sigma_1 J_1^3 + 3\sigma_2 J_1^2 J_2 + 3\sigma_3 J_1 J_2^2 + \sigma_4 J_2^3). \quad (5)$$

For this generating function, the twist is

$$\tau(J) = \tau_0 + \tau_1(J) = \begin{pmatrix} a & b \\ b & d \end{pmatrix} + \begin{pmatrix} \sigma_1 J_1 + \sigma_2 J_2 & \sigma_2 J_1 + \sigma_3 J_2 \\ \sigma_2 J_1 + \sigma_3 J_2 & \sigma_3 J_1 + \sigma_4 J_2 \end{pmatrix}. \quad (6)$$

The columns of τ_0, $(a,b)^T$ and $(b,d)^T$, are tangent to the images of the positive J axes at ω, and so define the opening angle of the frequency cone (recall Fig. 1). Vanishing of the twist at the origin occurs if the columns of τ_0 are parallel or antiparallel. If the vectors are parallel, the frequency cone collapses at the twistless point, and if they are antiparallel, it opens to 180°. To next order in J, the boundaries of this cone are parabolas whose symmetry axes are given by the vectors $(\sigma_1, \sigma_2)^T$ and $(\sigma_3, \sigma_4)^T$. Depending upon the orientation of these vectors, the cone boundaries are curved either toward its interior or its exterior. These then determine whether the frequency map is locally one-to-one when $\det \tau_0$ is positive or negative.

Finally, the twist could vanish if both elements in one column of τ_0 are zero, i.e., when the kernel of τ_0 coincides with a coordinate axis. Since this requires two conditions on τ_0, it is codimension-two. This corresponds to the transition between the parallel and antiparallel cases.

The critical set, $\det \tau = 0$, for (6) is a quadratic curve. When the curve is an ellipse, its caustic contains three cusps, and when it is a hyperbola one branch of the caustic is a fold and the other has a single cusp. Since we consider a power series about the origin, we are most interested in the singularities when they occur at the image of $J=0$ which is $\Omega = \omega$. From (4), there is a cusp at ω when

$$\delta(0) = a(3b\sigma_3 - a\sigma_4) - b(3b\sigma_2 - d\sigma_1) = 0.$$

Otherwise, the image of the origin is a fold point. We will primarily study folds in this article, leaving the study of cusps to a later work,[25] so we assume that $\delta(0) \neq 0$.

The fold can cross $J=0$ in two ways, depending upon the slope of the critical set at the origin:

$$m = -\frac{d\sigma_1 + a\sigma_3 - 2b\sigma_2}{d\sigma_2 + a\sigma_4 - 2b\sigma_2}.$$

If m is negative, then as $\det \tau_0$ crosses zero the fold line appears to be created or destroyed at the origin, since it moves through the nonphysical negative J quadrants into the first quadrant. However, if the fold has positive slope, then there will be a nearby fold for both signs of $\det \tau_0$.

We show the four possible cases in Figs. 2–5. The columns of τ_0 pass through the parallel state in Figs. 2 and 3, and the antiparallel state in Figs. 4 and 5. When the slope of the critical set is positive as in Figs. 2 and 4, the fold curve is present on both sides of $\det \tau_0 = 0$, but it intersects the image of the J_1 axis on one side and the J_2 axis on the other. When the slope is negative as in Figs. 3 and 5, the fold is present in the image of the positive quadrant only when $\det \tau_0 < 0$.

III. ELLIPTIC FIXED POINTS

Suppose $f: \mathbb{R}^{2d} \to \mathbb{R}^{2d}$ is a symplectic map and $z = f(z)$ is a fixed point. We call the eigenvalues of $Df(z)$ its "multipliers," and denote them by μ_i. Since Df is a symplectic matrix, its multipliers come in reciprocal pairs $\{\mu_k, 1/\mu_k, k = 1,...,d\}$, and the corresponding eigenvectors span a two-dimensional symplectic subspace. We define traces in each symplectic subspace as

$$\rho_k = \mu_k + 1/\mu_k,$$

and the residues[26] as

$$R_k = \tfrac{1}{4}(2 - \rho_k). \quad (7)$$

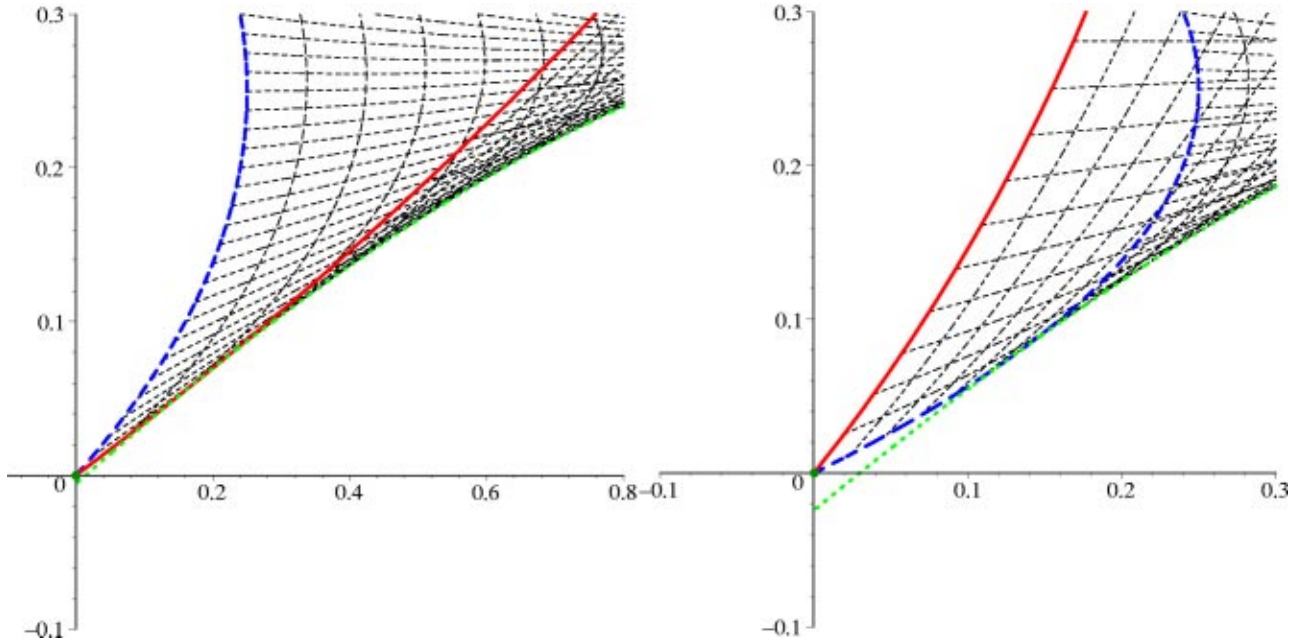

FIG. 2. (Color online) A frequency map when the columns of τ pass through the parallel state and the critical curve has positive slope. Here $\omega=(0,0)$ and $\sigma=(-1,1,-2,0)$. For the left panel $\tau=[(3,1)^T,(1,0.5)^T]$, and for the right panel, $\tau=[(0.8,1)^T,(1,0.5)^T]$. The grid of thin curves is the image of the positive quadrant which is bounded by the images of the J_1-axis (solid), and the J_2-axis (dashed). The caustic (dotted curve) intersects the image of the J_1-axis when $\det \tau_0>0$, and the J_2-axis when the orientation reverses.

When $0\leqslant R_k\leqslant 1$, the multiplier μ_k is on the unit circle. We assume, more strongly, that $0<R_k<1$ and $R_k\neq R_j$, for $k\neq j$. In this case the origin is a linearly stable fixed point; it is called ''strongly-stable'' following Arnold.[1] This excludes the saddle-center and period-doubling bifurcation values $\mu=\pm 1$, and the Krein collisions $\mu_k=\mu_j$. Though a fixed point may be linearly stable at these resonant points, it is not generally so.

For an elliptic fixed point, we define the rotation vector $\omega\in\mathbb{R}^d$ by

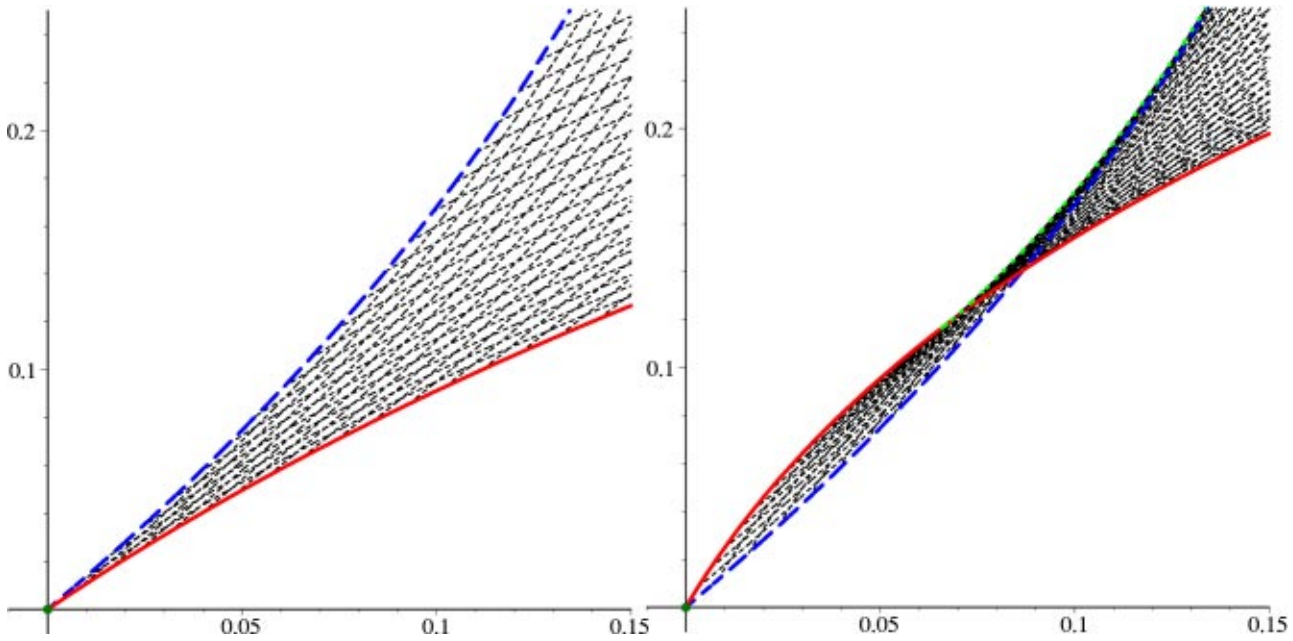

FIG. 3. (Color online) A frequency map when the columns of τ pass through the parallel state and the critical curve has negative slope. Here $\omega=(0,0)$ and $\sigma=(3,-1.5,-3,1.5)$. For the left panel $\tau=[(1,1.1)^T,(1.1,1.55)^T]$, so that $\det \tau>0$, and for the right panel $\tau=[(0.4,1.1)^T,(1.1.55)^T]$, so that $\det \tau<0$. The critical set enters the positive quadrant when $\det \tau<0$ and intersects both boundaries of the cone, thus the caustic (dotted curve) is only visible in the right panel.

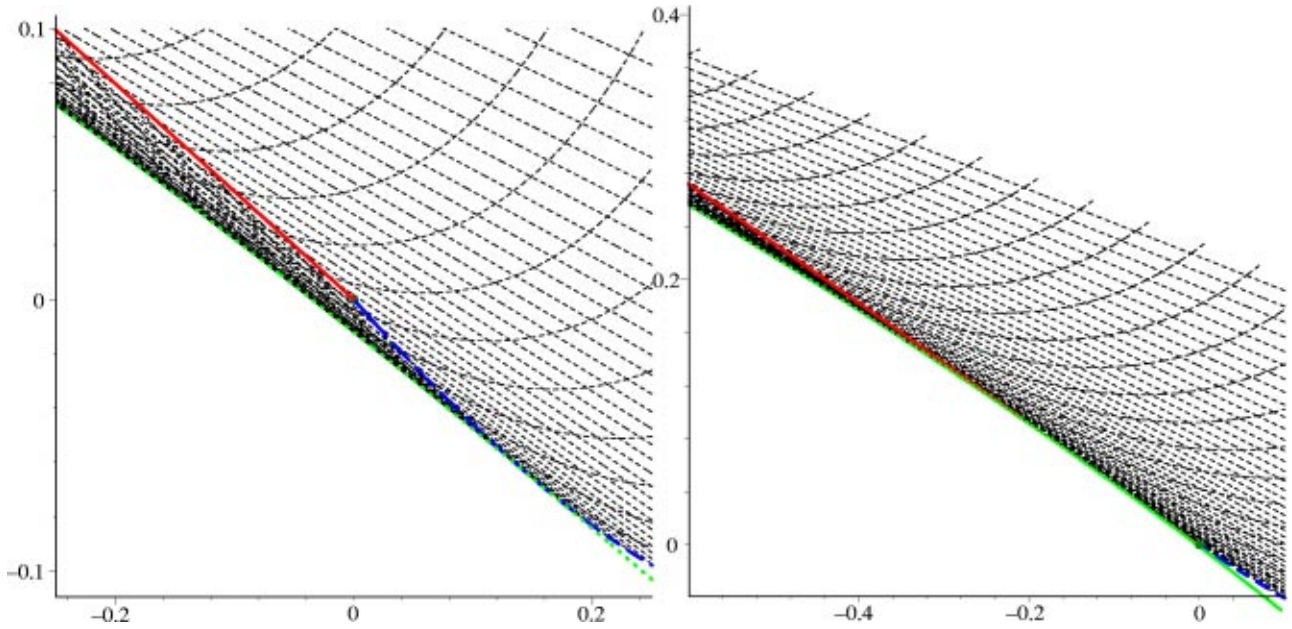

FIG. 4. (Color online) A frequency map when the columns of τ pass through the antiparallel state and the slope of the critical curve is positive. Here $\omega=(0,0)$ and $\sigma=(-0.3,0,-0.5,1)$. For the left panel $\tau=[(0.8,1.15)^T,(1.15,0.5)^T]$, and for the right panel, $\tau=[(0.8,1)^T,(1,0.5)^T]$. For positive orientation, the caustic crosses the image of the J_2 axis; and when the orientation reverses, it crosses the J_1 image.

$$\mu_k = e^{2\pi i\omega_k}, \quad k=1,...,d. \tag{8}$$

Since the multipliers come in reciprocal pairs, we can always choose $\omega_k \in (0,\frac{1}{2})$, for then the reciprocal multiplier corresponds to negative rotation number. With this convention, the traces, $\rho_k = 2\cos 2\pi\omega_k$ and the residues,

$$R_k = \sin^2 \pi\omega_k = \tfrac{1}{4}|\mu_k - 1|^2, \tag{9}$$

are one-to-one in ω_k.

A. Kinematics of resonances

In the neighborhood of an elliptic fixed point, a map can be transformed into the Birkhoff normal form (1) to arbitrary order whenever it is not resonant. A resonance corresponds to an integer vector $m=(m_1,\ldots,m_d)\in\mathbb{Z}^d$ such that

$$\mu^m \equiv \mu_1^{m_1}\mu_2^{m_2}\cdots\mu_d^{m_d} = 1. \tag{10}$$

Using 8, this is equivalent to the existence of $n\in\mathbb{Z}$ such that

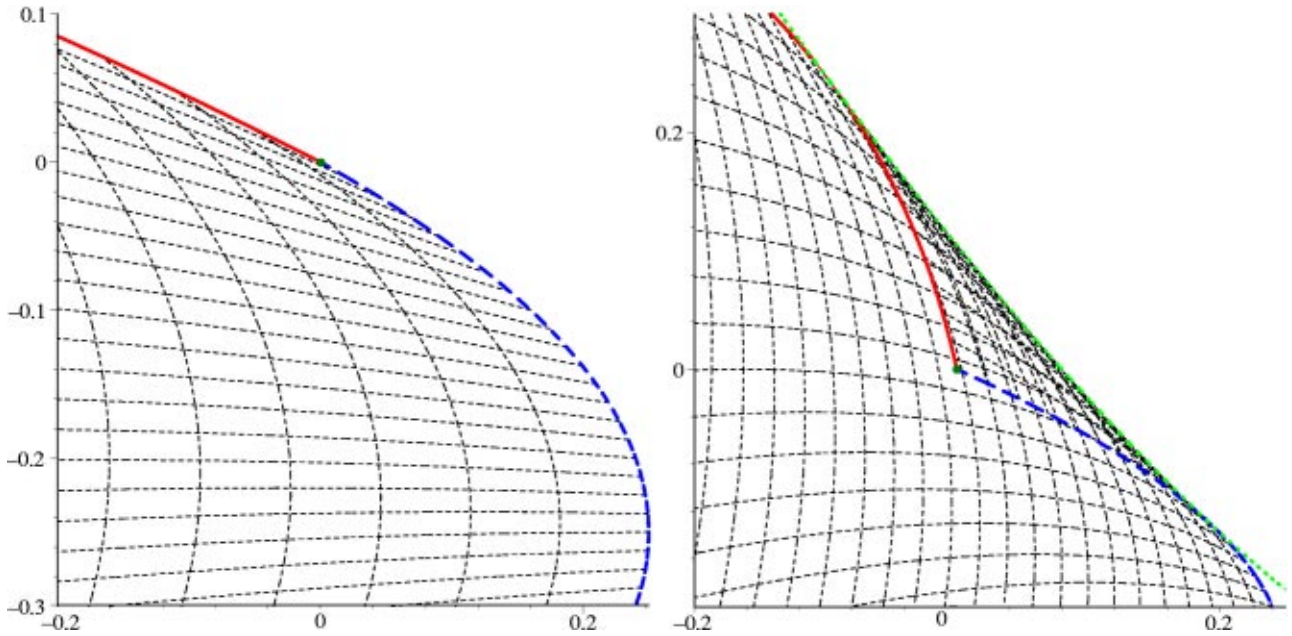

FIG. 5. (Color online) A frequency map when the columns of τ pass through the antiparallel state and the slope of the critical curve is negative. Here $\omega=(0,0)$ and $\sigma=(-1,-1,-2,0)$. For the left panel $\tau=[(-2.2,1)^T,(1,0.5)^T]$ and the caustic is not visible. For the right panel $\tau=[(-0.2,1)^T,(1,-0.5)^T]$ has negative determinant and a fold is present.

$$m\cdot\omega = n. \tag{11}$$

Thus, in frequency space, a resonance corresponds to a codimension-one plane, and the set of all resonances is the set of planes with integral normal vectors, m, and rational intercepts with the coordinate axes. Thus, the collection of resonances can be labeled by vectors $(m,n)\in\mathbb{Z}^{d+1}$.

Since (11) is homogeneous in (m,n), we can assume that the components of this vector are coprime without loss of generality. However, we need not consider all such vectors. Two resonances are equivalent if they can be transformed into one another by $\omega' = \omega - l$, where $l\in\mathbb{Z}^d$. The corresponding action on the resonance is $n\to n' = n - l\cdot m$. Similarly, resonances are equivalent if they can be transformed into one another by $\omega' = -\omega$, which induces the action $n\to n' = -n$. A well known lemma[27] implies that there exists an integer vector $l\in\mathbb{Z}^d$ such that $0\leqslant n' < \gcd(m)$. In particular, if the components of m are coprime, then n can always be chosen to be 0, since $\gcd(m)=1$.

Since $\rho_i = 2\cos(2\pi\omega_i)$, the resonance condition can be written in terms of the traces as

$$\sum_{i=1}^{d} m_i \arccos(\rho_i/2) = 2\pi n. \tag{12}$$

Generally this equation can be transformed into a polynomial in the traces by using Chebyshev polynomials

$$T_m(\rho/2) \equiv \cos(m\arccos(\rho/2)). \tag{13}$$

Since $\rho\in[-2,2]$ when the fixed point is elliptic, this polynomial is real.

B. Resonances for four-dimensional maps

For $d=2$, we can convert the resonance condition (12) to polynomial form simply by moving the second term to the right-hand side and taking the cosine of both sides. This gives the polynomial

$$\mathcal{R}_{m_1m_2} = T_{m_1}(\rho_1/2) - T_{m_2}(\rho_2/2),$$

whose zeros correspond to the (m_1,m_2,n) resonances. Note that n has vanished from this form, as it must, since n does not appear in (10). Moreover, it is clear from this form that the signs of the m_i are irrelevant since $T_m(x) = T_{-m}(x)$. This can also be seen by noting that the traces involve the multiplier and its reciprocal symmetrically and so do not depend upon whether μ or μ^{-1} is involved in the condition (10). The first few resonance polynomials, written as functions of the residues, are

$$\begin{aligned}
\mathcal{R}_{10} &= -2R_1,\\
\mathcal{R}_{11} &= -2(R_1 - R_2),\\
\mathcal{R}_{20} &= 8R_1(R_1-1),\\
\mathcal{R}_{21} &= 8R_1(R_1-1) + 2R_2,\\
\mathcal{R}_{30} &= -2R_1(4R_1-3)^2.
\end{aligned} \tag{14}$$

If the vector m is reducible, i.e., $\gcd(m_1,m_2)\neq 1$, then the polynomials $\mathcal{R}_m$ can be factored. This follows from the relation

$$T_{km}(x) = T_k(T_m(x)),$$

which is a simple consequence of the definition (13). In particular, note that if $m_1 = km_1'$ and $m_2 = km_2'$, then

$$T_{m_1}(x) - T_{m_2}(y) = T_k(T_{m_1'}(x)) - T_k(T_{m_2'}(y)),$$

and since the polynomial equation $p(x)-p(y)$ always has a factor $x-y$, we can write

$$\mathcal{R}_{m_1m_2} = P(R_1,R_2)\mathcal{R}_{m_1'm_2'},$$

where P is a polynomial of degree $(k-1)\max(m_1',m_2')$. This process can be repeated for each common factor in the components of m. When this is completed, each of the factors corresponds to a particular value of n; since they will appear as denominators in the Birkhoff normal form, we denote these by $\mathcal{D}_{m_1m_2n}$. When m is coprime, then $n=0$ so that $\mathcal{D}_{m,0}\propto\mathcal{R}_m$, but we adjust the sign and divide out inessential constants. Here are the first few cases:

$$\begin{aligned}
\mathcal{D}_{201} &= 1 - R_1;\\
\mathcal{D}_{021} &= 1 - R_2;\\
\mathcal{D}_{301} &= 4R_1 - 3;\\
\mathcal{D}_{031} &= 4R_2 - 3;\\
\mathcal{D}_{210} &= 4R_1(R_1-1) + R_2;\\
\mathcal{D}_{120} &= 4R_2(R_2-1) + R_1.
\end{aligned} \tag{15}$$

To plot the resonance curves in the trace or residue space, we can use parametric curves. For example, if $m_2 \neq 0$, the (m,n) resonance is the curve

$$\omega_1 = tm_2, \quad \omega_2 = -tm_1 + \frac{n}{m_2}.$$

Using the definition of the traces, this gives the curves

$$\rho_1(t) = 2\cos(2\pi m_2 t),$$

$$\rho_2(t) = 2\cos\left(2\pi m_1 t - 2\pi\frac{n}{m_2}\right).$$

Therefore the resonant curves in the space of traces or residues are Lissajous figures.

In the left panel of Fig. 6 we show the resonance curves up to order four. The right panel of the figure shows resonances up to order 9. While this picture may seem similar to the familiar ''Arnold web'' of resonances in action space,[28] it represents resonances at the fixed point in the parameter space of a family of maps and not resonances in the space of initial conditions (e.g., actions) of one map.

IV. QUADRATIC SYMPLECTIC MAPS

Here we will illustrate the formation of twist singularities by studying a four-dimensional quadratic, symplectic map that has a strongly-stable, elliptic fixed point. The general form for quadratic symplectic maps has been found by Moser,[29] generalizing Hénon's quadratic map[30] to higher dimensions. Since this map does not necessarily have fixed

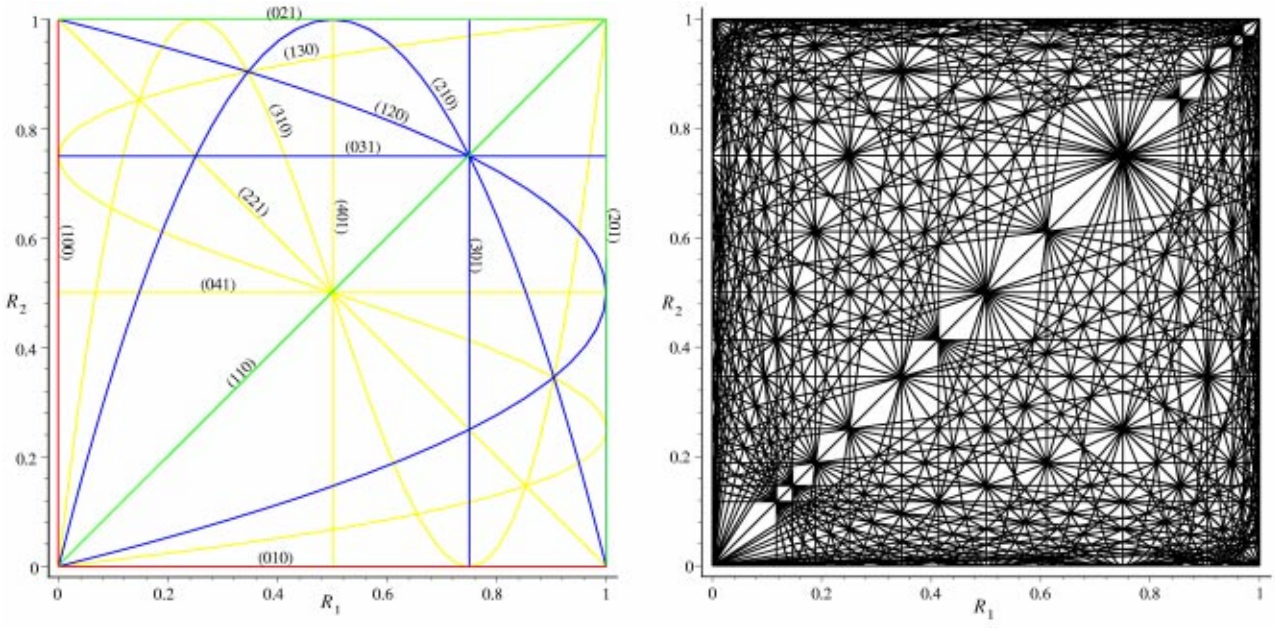

FIG. 6. (Color online) Resonances curves up to order 4 (left panel) and order 9 (right panel) in the space of residues.

points, we start with that assumption to construct our example. In the Appendix we will show how to obtain our map from Moser's general quadratic map.

We will use a Lagrangian generating function to write our map in "standard" form,

$$L(x,x')=K(x'-x)-V(x), \tag{16}$$

where K is the "kinetic" and V is the "potential" energy. The map is generated via the one form $y'dx'-ydx=dL$, giving

$$\begin{aligned} y&=-\frac{\partial L}{\partial x}=DK(x'-x)+DV(x),\\ y'&=\frac{\partial L}{\partial x'}=DK(x'-x). \end{aligned} \tag{17}$$

If this map has a fixed point, then we can shift it to the origin. The new generating function then has no linear terms in V.

First we consider the quadratic Lagrangian when there is a strongly-stable fixed point at the origin. In this case coordinates in phase space can be chosen so that the map is in real block diagonal normal form (see, e.g., Ref. 2). Such a map is generated by a quadratic Lagrangian of the form

$$L^{(2)}(x,x')=\sum_{k=1}^{d}\frac{s_k}{2}[(x_k'-x_k)^2-4R_kx_k^2]. \tag{18}$$

Here the R_k are the residues of the fixed point, and the $s_k=\pm 1$ are signs that determine the Krein signature—effectively the direction of rotation in each canonical plane. The quadratic Lagrangian (18) generates the linear map with matrix

$$M=\mathrm{diag}\left[\begin{pmatrix} 1-4R_k & s_k\\ -4R_ks_k & 1\end{pmatrix},k=1,\ldots,d\right]. \tag{19}$$

This is easily seen to be equivalent to the more common rotation matrix form.[2] The matrix M can be written as $M=B^{-1}M'B$ where M' is the symplectic rotation with diagonal blocks

$$M_k'=\begin{pmatrix} \cos 2\pi\omega_k & s_k\sin 2\pi\omega_k\\ -s_k\sin 2\pi\omega_k & \cos 2\pi\omega_k\end{pmatrix},$$

and B is symplectic with the blocks

$$B_k=\frac{1}{\sin(2\pi\omega_k)}\begin{pmatrix} 0 & 1\\ -\sin(2\pi\omega_k) & 2s_kR_k\end{pmatrix}.$$

Now we want to consider nonlinear perturbations of this strongly-stable fixed point. We represent the quadratic nonlinear terms in the map by adding a cubic potential to the generating function,

$$V^3(x)=\sum_{i+j=3}a_{ij}x_1^ix_2^j. \tag{20}$$

The standard map generated by (16) with $V(x)=\Sigma 2s_kR_kx_k^2+V^{(3)}(x)$ and $K(v)=\Sigma s_kv_k^2/2$ is

$$\begin{aligned} x_k'&=x_k+s_ky_k',\\ y_k'&=y_k-4R_ks_kx_k-D_kV^{(3)}(x). \end{aligned} \tag{21}$$

A special case of this system is the "natural map" obtained when the Krein signatures s_k are equal. In this case, the definiteness of the kinetic energy imposes some restrictions on the behavior of the system.[31]

Note that the inverse of the map (21) is easy to obtain:

$$\begin{aligned} x_k'&=x_k-s_ky_k,\\ y_k'&=y_k+4R_ks_kx_k'+D_kV^{(3)}(x'). \end{aligned}$$

Thus (21) is a polynomial diffeomorphism and has a polynomial inverse of the same degree.

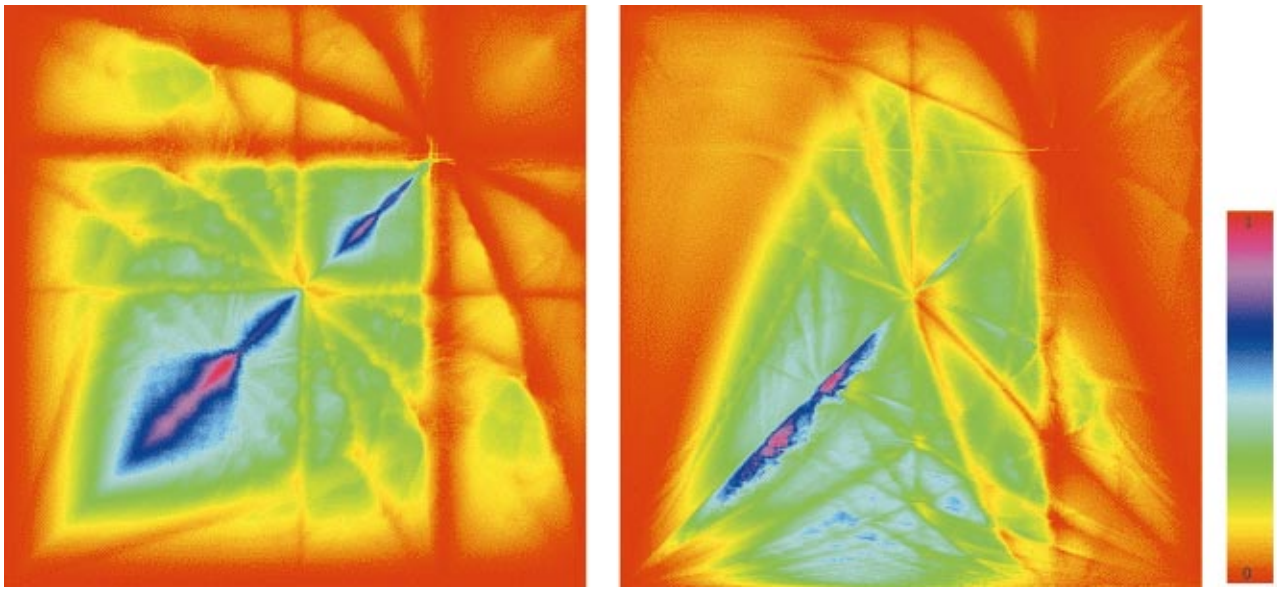

FIG. 7. (Color) Estimated size of the island of quasiperiodic motion around the elliptic fixed point of the cubic natural map as a function of the residues using the area of trapped orbits on the symmetry plane. We choose $s_1=s_2$, and for the left panel set $a_{ij}=0.1$ while for the right $a_{30}=a_{21}=0$. The trapped area is indicated with the hue on the color wheel, with red (0°) corresponding to the smallest island, through green to blue to magenta (359°) as the largest.

A. Island size

The map (21) has rich dynamical behavior which has only been partially explored. One experiment that illustrates some of the phenomena is the computation of the size of the stable island around the elliptic fixed point. For the two-dimensional case this experiment was first performed by Hénon.[30] Those calculations clearly showed the strong dependence of the size of the island on the residue, and in particular that it shrinks to zero at the $\omega=\frac{1}{3}$ resonance. Hénon used the length of the portion of the symmetry line that contains bounded orbits as an estimate for the area of the island. The actual area of the island can also be computed by ''counting pixels'' that contain trapped initial conditions,[32] or by the more efficient and precise method of exit time distributions.[22]

The quadratic map (21) does have reversing symmetry with a fixed set $\{x=0\}$. Thus, by analogy with Hénon's work we can estimate the trapped volume by looking only at initial conditions starting on this symmetry plane and estimating the area for which the trajectories are bounded. In Fig. 7 the results are shown for two different set of parameters. To determine the trapped island area in the symmetry plane we assume that the region is star convex and calculate its area by dissecting it into 100 equal sectors. For each ray bounding a

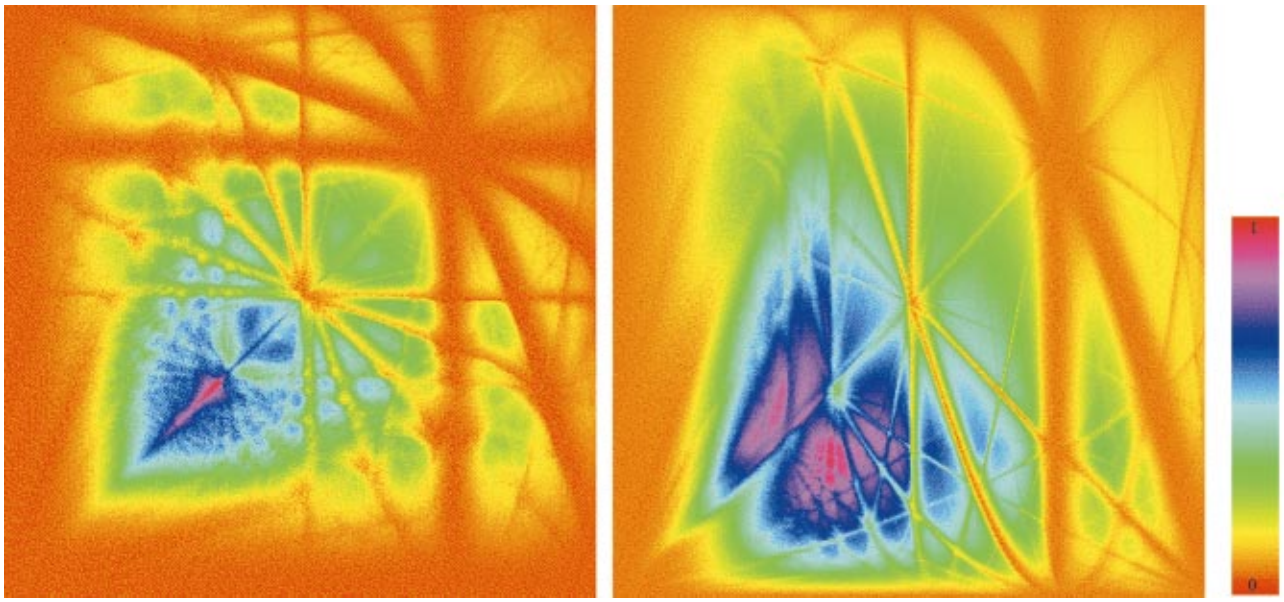

FIG. 8. (Color) Estimated volume of bounded orbits in the island of quasiperiodic motion around the elliptic fixed point of the cubic natural map as a function of the residues using the average exit time. Parameters are the same as in Fig. 7.

sector the boundary of the island is estimated by considering an orbit as trapped if it does not leave the cube of bounded orbits for 1000 iterations. The transition point on each ray is found by bisection. This is much more efficient than counting pixels would be, particularly for large islands, though it does rely on the assumption of star convexity.

We observe that the island size is strongly influenced by the low order resonances. In the left panel, the area shrinks to zero near and outside the (301) and (031) resonances, while in the right panel the (210) resonance is most effective. Many of the resonances shown in Fig. 6 are visible in particular in the right picture. The fact that the (110) resonance increases the island size (instead of decreasing it) is related to the fact that under the strong-stability assumption, our map is diagonalizable when $\omega_1 \to \omega_2$; generically, this would not be the case, and the (110) resonance might have a strong effect in the opposite way.

For four-dimensional maps an explicit volume calculation by counting ''voxels'' is prohibitively expensive; however, the exit time distribution technique[22] is much more efficient and can still be carried out. To do this, we choose a hypercube $\mathcal{C}=\{|x|,|y|<2\}$ that appears to contain all of the bounded orbits. Moser[29] gives a larger box that contains all bounded orbits, but from our numerical experiments we see that for our parameters $\mathcal{C}$ is sufficient. The incoming set for $\mathcal{C}$ is the portion of the cube that is not in its image, $\mathcal{I}=\mathcal{C}\backslash f(\mathcal{C})$. The exit time, $t^+(z)$ for a point $z\in\mathcal{I}$, is the number of iterations until it leaves $\mathcal{C}$, and the average exit time, $\langle t^+\rangle_{\mathcal{I}}$, is the average over all points in $\mathcal{I}$. If we compute this average, then the volume of the accessible region is given by $\langle t^+\rangle_{\mathcal{I}}\mu(\mathcal{I})$. Thus the volume of trapped orbits is $\mu(\mathcal{C})-\langle t^+\rangle_{\mathcal{I}}\mu(\mathcal{I})$, where μ is the measure of the respective sets.

The exit time computation is realized as a Monte Carlo simulation. First pick a random point in the cube $\mathcal{C}$. If its preimage is in $\mathcal{C}$, then it is not in $\mathcal{I}$, and it is discarded; otherwise, determine the exit time of the point. The average over all such points is $\langle t^+\rangle_{\mathcal{I}}$. The probability P_I of a point to be in I gives $\mu(\mathcal{I})\approx P_I\mu(\mathcal{C})$. In this Monte Carlo realization, statistical fluctuations can give an accessible volume slightly larger than $\mu(\mathcal{C})=4^4$. In this case the trapped area is set to be 0.

Typical results are shown in Fig. 8, for the same parameters as in Fig. 7. The results are qualitatively similar to the previous one, though the volume drops more dramatically near higher order resonances than the area on the symmetry plane does, presumably because volume has sampled new regions of phase space.

B. Normal form

To transform (21) to Birkhoff normal form it is convenient to use complex coordinates that diagonalize the linearization. Each block of (19) has eigenvalues μ_k and $\overline{\mu_k}$, and eigenvectors $v_k=(1/f_k)\begin{pmatrix}1\\ s_k(1-\overline{\mu_k})\end{pmatrix}$ and $\overline{v_k}$, for some normalization given by f_k. Complex coordinates $(z,\overline{z})$ can be introduced so that the new system is diagonal by defining

$$\begin{pmatrix}x_k\\ y_k\end{pmatrix}=v_k z_k+\overline{v_k}\,\overline{z_k}. \tag{22}$$

The normalization of v_k is arbitrary; because the nonlinear terms in the map are only functions of x_k, we choose it so that the relation $x_k=(1/f_k)(z_k+\overline{z_k})$ is simple, i.e., so that f_k is real and positive. Since the Poisson brackets of the old and new variables are related by $1=\{x_k,y_k\}=v_k\times\overline{v_k}\{z_k,\overline{z_k}\}$, this means that the cross product of the eigenvectors must be imaginary and depends upon the Krein signature. We choose the normalization so that

$$\{z_k,\overline{z_k}\}=2is_k,$$

which implies that $v_k\times\overline{v_k}=-(i/2)s_k$, and gives

$$f_k=2\sqrt{\sin 2\pi\omega_k}=2\sqrt{2}(R_k(1-R_k))^{1/4}. \tag{23}$$

Note that f_k is real and nonzero because of the convention that $0<\omega<\frac{1}{2}$. The inverse of the transformation (22) can be written

$$z_k=\frac{2i}{f_k}[(1-\mu_k)x_k-s_k y_k]. \tag{24}$$

In these coordinates (21) is transformed into

$$z_k'=\mu_k\left[z_k+\frac{2is_k}{f_k}D_k V^{(3)}\left(\frac{z+\overline{z}}{f}\right)\right], \tag{25}$$

together with the corresponding complex conjugate equations. Here $D_j V^{(3)}(x)$ denotes the derivative of the nonlinear terms in the potential with respect to the jth argument, i.e., x_j.

It is interesting that the sole effect of the Krein signatures in (25) is to modify the signs of the terms in the gradient of the potential. Of course, when we transform back to real variables, (24) shows that the direction of rotation depends upon s_k as well.

Since $V^{(3)}$ is a polynomial, each nonlinear term in the complex map (25) has the form of a constant times $z^j\equiv\Pi_{k=1}^d z_k^{j_k}\overline{z_k}^{\overline{j_k}}$ where the exponents are all non-negative integers. The degree of the term is $J=\Sigma_{k=1}^d j_k+\overline{j_k}$. In its simplest form, the Birkhoff normalization of (25) proceeds iteratively to attempt to remove each term of degree $J>1$ in the map using a coordinate transformation of the form $\zeta=z+Z(z,\overline{z})$, where Z is a vector of homogeneous polynomials of degree J. We start with $J=2$ to remove the quadratic terms, and then proceed successively to remove cubic terms and so forth.

In order to remove a particular term z^j of degree J in the map for z_i', we require a term in Z_i with coefficient proportional to $(\Pi_{k=1}^d \mu_k^{j_k}\overline{\mu_k}^{\overline{j_k}}-\mu_i)^{-1}$. Since $\overline{\mu}=1/\mu$ the transformation exists as long as

$$\prod_{k=1}^{d}\mu_k^{j_k-\overline{j_k}}\neq\mu_i.$$

Thus, for the case $d=2$ and a resonance $\mu^m=1$, the transformation does not exist for the z_i' component when

$$\begin{aligned} &i=1\ :\ nm_1=j_1-\overline{j_1}-1,\quad nm_2=j_2-\overline{j_2},\\ &i=2\ :\ nm_1=j_1-\overline{j_1},\quad nm_2=j_2-\overline{j_2}-1, \end{aligned} \tag{26}$$

with some nonzero integer n.

For certain terms this will give $m_1=m_2=0$, in which case the corresponding term can never be removed by a coordinate transformation. The coefficients of these irremovable terms are called the twists. In the present case up to degree 3 they are given by z_1, $z_1(z_1\overline{z_1})$, $z_1(z_2\overline{z_2})$ for the z_1' equation and by z_2, $z_2(z_1\overline{z_1})$, $z_2(z_2\overline{z_2})$ for the z_2' equation. The transformation to normal form has to remove all the quadratic terms (if nonresonant). There are ten of them, so the transformation has ten corresponding terms to remove them. Assuming that all the other terms of degree 3 can be removed (i.e., assuming there is no resonance up to including order 4), the map takes the form

$$\zeta_k'=\mu_k\zeta_k\left(1+i\pi s_k\sum_{j=1}^{d}\tau_{kj}|\zeta_j|^2\right) \tag{27}$$

plus terms of degree 4 or higher in ζ.

Introducing action-angle variables (J,θ) by $\zeta_k=\sqrt{2J_k}e^{is_k\theta_k}$ gives the standard form of a twist map

$$\begin{aligned} J_k'&=J_k,\\ \theta_k'&=\theta_k+2\pi\left(s_k\omega_k+\sum_{j=1}^{d}\tau_{kj}J_j\right), \end{aligned} \tag{28}$$

plus terms of degree 2 or higher in J and periodic in θ. The twist matrix is symmetric because the map is symplectic.

The three entries of the symmetric twist-matrix τ_{jk} for the cubic map are given by

$$\begin{aligned} \tau_{11}&=\frac{1}{64\pi R_1\mathcal{D}_{201}}\left(9a_{30}^2s_1\frac{5-8R_1}{R_1\mathcal{D}_{301}}+a_{21}^2s_2\frac{\mathcal{N}_{12}}{R_2\mathcal{D}_{210}}\right),\\ \tau_{22}&=\frac{1}{64\pi R_2\mathcal{D}_{021}}\left(9a_{03}^2s_2\frac{5-8R_2}{R_2\mathcal{D}_{031}}+a_{12}^2s_1\frac{\mathcal{N}_{21}}{R_1\mathcal{D}_{120}}\right),\\ \tau_{12}&=\frac{1}{16\pi\sqrt{R_1R_2\mathcal{D}_{201}\mathcal{D}_{021}}}\left(a_{21}^2s_1\frac{\mathcal{N}_1}{\mathcal{D}_{210}}+a_{12}^2s_2\frac{\mathcal{N}_2}{\mathcal{D}_{120}}\right.\\ &\quad\left.-a_{12}a_{30}s_1\frac{3}{2R_1}-a_{21}a_{03}s_2\frac{3}{2R_2}\right), \end{aligned} \tag{29}$$

where the resonance denominators are given in (15) and the numerators by

$$\begin{aligned} \mathcal{N}_{jk}&=8R_j(1-R_j)-3R_k,\\ \mathcal{N}_k&=1-2R_k. \end{aligned}$$

It is of course no accident that the resonance polynomials appear as the denominators of the corresponding resonant terms.

The relation between the exponents $j_k,\overline{j_k}$, the resonances m and the resonance curves in residue space (recall Fig. 6) is interesting. On the one hand, starting with given exponents, there can be more than one (but finitely many) resonances corresponding to them. Whether the resonance is important depends of course on its amplitude. On the other hand, a given resonance curve accounts for a number of resonances and an infinite number of corresponding exponents.

The truncated nonresonant normal form has the two actions $J_k=\zeta_k\overline{\zeta_k}/2$ as integrals. Transforming back to the original coordinates x and y gives cubic approximations for the integrals

$$\begin{aligned} \frac{1}{2}f_1^2J_1&=4R_1x_1(x_1-s_1y_1)+y_1^2-\frac{3s_1a_{30}}{\mathcal{D}_{301}}x_1(2x_1-s_1y_1)\\ &\quad\times(x_1-s_1y_1)-\frac{s_1a_{21}}{\mathcal{D}_{210}}(2R_1(2x_2-s_2y_2)x_1^2\\ &\quad-s_1(4R_1x_2-s_2y_2)x_1y_1+(2R_1-1)x_2y_1^2)\\ &\quad+\frac{s_1a_{12}}{\mathcal{D}_{120}}((R_1-2R_2)(2x_1-s_1y_1)x_2^2+s_2(2(2R_2\\ &\quad-R_1)x_1-s_1(2R_2-1)y_1)x_2y_2+(R_1-1)x_1y_2^2)\\ &\quad+O(4). \end{aligned} \tag{30}$$

The first three terms contain the expression from a cubic, two-dimensional map while the remaining terms give the result of the coupling proportional to a_{21} and a_{12} (the term a_{03} does not enter to this order). The analogous equation for J_2 is obtained by exchanging the indices 1 and 2 and also 0 and 3.

V. FOLD SINGULARITIES NEAR AN ELLIPTIC FIXED POINT

The twist coefficients of the Birkhoff normal form can be used to find singularities of the frequency map. When $\det\tau_0$ is zero, there is a singularity at the fixed point that we call a twistless bifurcation. Since we are not able to determine whether this bifurcation is a fold or a cusp without calculating τ_1, we will focus on the fold case. We show in this section that a fold singularity necessarily occurs in one-parameter families of maps, if the family crosses a tripling resonance line in a certain way.

A. Twistless curves

As we discussed in Sec. II C, the type of twistless bifurcation obtained when a fold crosses the origin depends upon whether the columns of τ_0 are parallel or antiparallel. To visualize this, consider the two direction fields given by the normalized column vectors of τ_0. We show these fields in Fig. 9 for two sets of values for the nonlinear parameters a_{ij}; since the components of τ_0 are homogeneous quadratic polynomials in these parameters, their overall scale is unimportant and there are only three independent parameters that determine this direction field in residue space. Thus we can specify only the ratios of the values of the a_{ij} to define the picture. In the figure, the first column vector of τ_0 corresponds to the black vectors and the second to the gray vectors.

Notice that the twist vectors in the figure appear to be either nearly aligned or antialigned over a large region near $R_1=R_2\approx0.5$, but that their behavior varies rapidly near the resonance lines. Since $\det\tau_0=0$ is a single condition, we expect it to vanish on curves in the residue space. It is easy to obtain these curves numerically using a contour plotting algorithm; the plots are more easily constructed if we compute

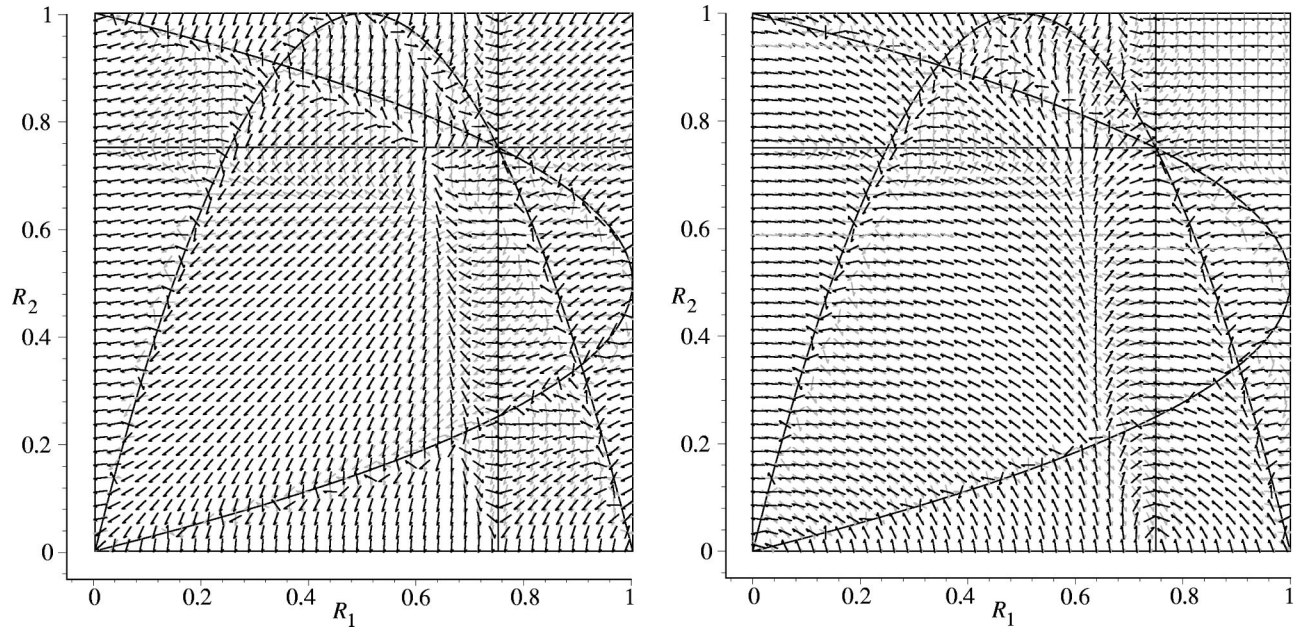

FIG. 9. Unit vector fields given by the columns of τ_0 as a function of the residues. The black and gray arrows represent the image of the J_1- and J_2-axes, respectively. We set $s_1=s_2$, for the left panel we choose $a_{30}=a_{21}=a_{12}=a_{03}$ and for the right panel $a_{30}=a_{21}=-2a_{12}=-2a_{03}$. Resonance curves up to order three are also shown. When the columns are parallel or antiparallel det τ_0 vanishes.

the numerator of the rational expression for det τ_0 from (29) and set it to zero, since this eliminates infinities which are unimportant in drawing the zeros. We show examples of these curves in Fig. 10 for the same parameter values as Fig. 9.

In general the expression for the twistless bifurcation curves in parameter space are quite complicated. However, the poles in det τ_0 that occur at low-order resonances are helpful in understanding the behavior, just as they were helpful in the two-dimensional case.[3] We will first obtain an elementary lemma about these poles, and then use it to prove a theorem about the necessity of twistless bifurcations in certain one-parameter families.

Lemma 1: *If all of the quadratic coefficients of the polynomial map (21) do not vanish, then the determinant of its twist has poles of order three at the* (100) *and* (010) *reso-*

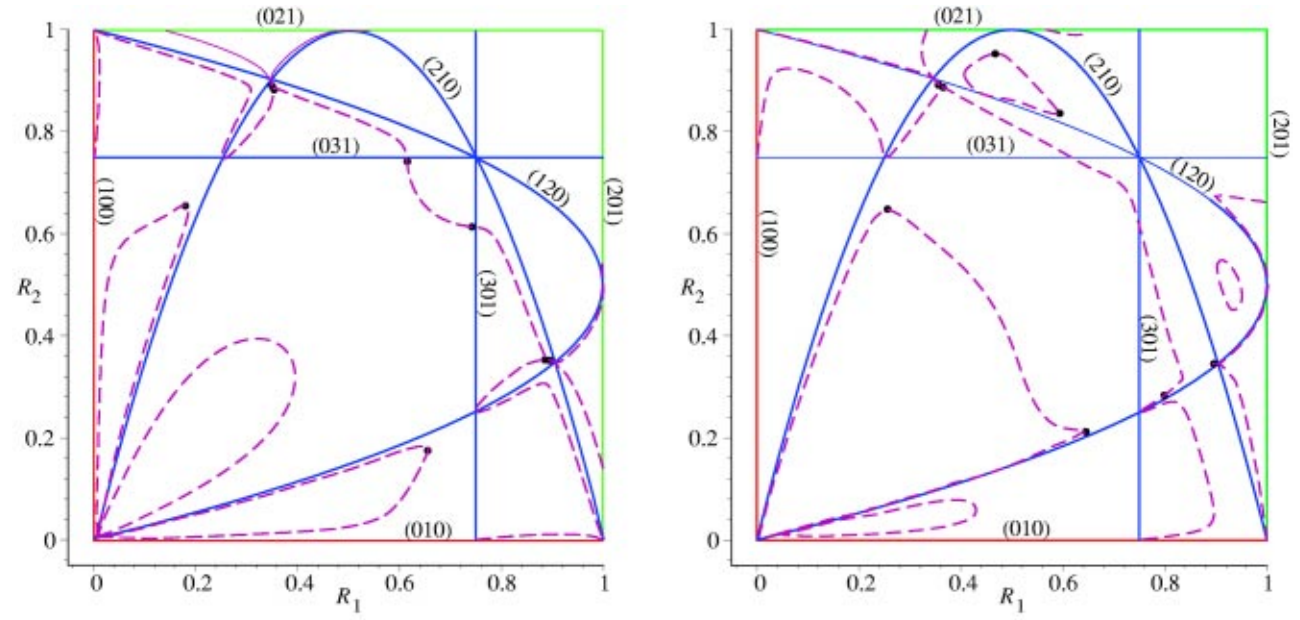

FIG. 10. (Color online) Resonance curves of orders 1, 2, and 3, and zeros of det τ_0 (dashed curves) in the residue space. Parameters are the same as Fig. 9. The dots indicate places where a column of τ_0 vanishes.

nances, poles of order two at the (210) *and* (120) *resonances and poles of order one at the* (201), (021), (301) *and* (031) *resonances. The coefficients of the second and third order poles are always negative.*

Proof: A straightforward expansion of $\det \tau_0$ near the (100) and (210) resonances gives

$$\det \tau_0 \sim -\frac{1}{R_1^3}\frac{3}{2048\pi^2}\frac{(a_{30}a_{12})^2}{R_2(1-R_2)}+\mathcal{O}(R_1^{-2}),$$

$$\det \tau_0 \sim -\frac{1}{\mathcal{D}_{210}^2}\frac{1}{1024\pi^2}\left(\frac{a_{21}^2}{R_1(1-R_1)}\right)^2+\mathcal{O}(\mathcal{D}_{210}^{-1}).$$

This gives the promised results for these resonances, since the denominators R_1 and $\mathcal{D}_{210}$ have first order zeros on the resonance curves. The expressions for the (010) and (120) resonances are obtained by exchanging coefficients $0\leftrightarrow 3$ and $1\leftrightarrow 2$ as usual. A similar calculation gives the expressions for the coefficients of the first order poles; these are complicated and not especially useful, so we do not give them explicitly. □

Since the second order poles have negative coefficients, twistless bifurcations are forced by the first order pole at the (301) and (031) resonances. However, which side of these resonance curves has the twistless curve depends upon the sign of the coefficient of the pole. Nevertheless we can conclude that there must be twistless bifurcations ''near'' the (301) and (310) resonances:

Theorem 2: *Suppose the map (21) has all of its quadratic coefficients a_{ij} nonzero. Let $\mathcal{P}$ be a path in residue space whose endpoints are on the* (210) *or* (120) *resonance curves and which transversely crosses either the* (310) or (301) *curve exactly once. Then there is a twistless bifurcation at some point on $\mathcal{P}$.*

Proof: Since $\mathcal{P}$ begins and ends on resonance curves where $\det \tau_0$ has a negative second order pole, then $\det \tau_0 < 0$ on $\mathcal{P}$ for points sufficiently close to its endpoints. Since there are poles of order 1 at the (310) and (031) resonances, it is necessary that $\det \tau_0 > 0$ when $\mathcal{P}$ approaches one side of these resonance curves. Thus $\det \tau_0$ crosses zero on $\mathcal{P}$. □

In Fig. 10, the twistless bifurcation that is forced by this mechanism is the curve that lies between the (301) line and the (210) parabola for small R_2, then crosses the (301) resonance near $R_2 = 0.6$, finally ending up between the (031) and (120) curves for small R_1. There may be other points where the twist vanishes as well—indeed in the figure several such curves occur—but the regions where they occur depend in detail on the parameter values as can be seen by comparing the two cases shown in Fig. 10.

Note that since the (210) resonance curve transversely crosses the (031) curve at the point $R=(\frac{1}{4},\frac{3}{4})$, corresponding to the frequencies $\omega=(\frac{1}{6},\frac{1}{3})$, the corollary implies that any small circle enclosing this point must contain at least two twistless points. Thus there must be a curve of twistless parameter values that goes through this double resonance. By symmetry, this is also true at the point $R=(\frac{3}{4},\frac{1}{4})$. We will investigate the structure of the frequency maps near this point below. A similar argument cannot be given for $R=(\frac{3}{4},\frac{3}{4})$, since here the four low-order resonance curves (210), (120), (310), and (130) all cross in such a way that small loops encircling this point do not cross the curves in the correct order to force twistless points.

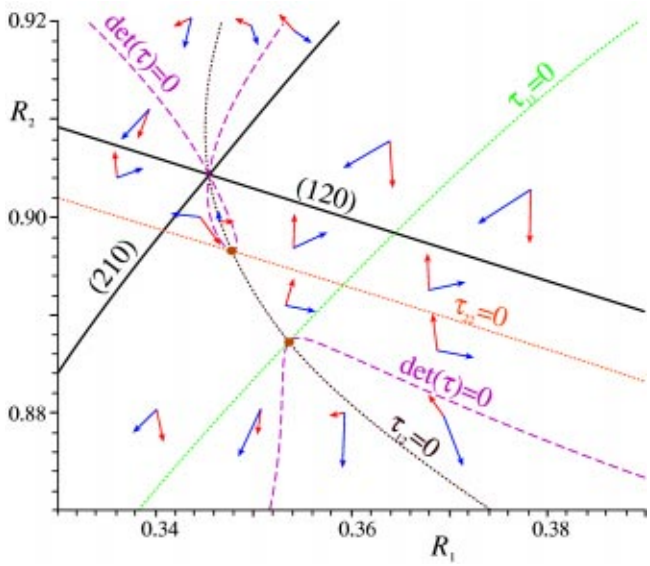

FIG. 11. (Color online) Enlargement of the left panel of Fig. 10 near the crossing of the (210) and (120) resonance curves (thick lines). The twistless curves (dashed) show a loop extending from this crossing point that was not visible in the previous figure. Also shown are the curves (dotted) along which individual components of the twist matrix vanish and dots at the codimension-two points.

As we move along a twistless curve in parameter space, it is possible for the twistless bifurcation to change from one of parallel type to one of antiparallel type. This can only occur when a column of the twist matrix vanishes, since the column vectors correspond to the tangent vectors of the images of the J axes (recall Fig. 1). Since vanishing of a column of τ requires two conditions, we expect this to occur at isolated points in the residue space: it is a codimension-two bifurcation. In Fig. 10 this occurs, for example, near the crossing of the (210) and (120) curves, corresponding to the double-resonance $\omega=(\frac{1}{5},\frac{2}{5})$. We show an enlargement of the left panel of Fig. 10 in Fig. 11. To show that a column of τ_0 vanishes along the twistless curves, we also plot the zero level sets of the three entries of the twist matrix in Fig. 11. There are two points on which a column of τ vanishes in this figure; the first column vanishes at $R\approx(0.3536,0.8874)$ and the second at $R\approx(0.3478,0.8965)$. Along the lower twistless curve in Fig. 11, the bifurcation is of antiparallel type to the right of the codimension-two point, and parallel to its left. All of the codimension-two points are indicated by the dots in Fig. 10.

All of the twistless curves in Fig. 10 correspond to the vanishing of a single eigenvalue of τ_0. In order that both eigenvalues of the symmetric twist matrix vanish, all three of the elements (29) must vanish simultaneously; thus this is a codimension-three phenomenon. We could achieve this by choice of one of the nonlinear terms in addition to the two residues. An easy place to search for this phenomenon is

close to the two neighboring codimension-two points corresponding to vanishing of each column of τ_0, e.g., near $R=(0.35,0.89)$ in Fig. 11. For example, if we allow a_{30} to vary from our standard choice of equal parameters, we find that the matrix τ_0 vanishes identically when $R \approx (0.348\,41, 0.896\,33)$ and $a_{30}=1.526\,63a_{21}$. This corresponds to a simultaneous ''crossing'' of the three curves of zero twist matrix entries; this is not a persistent crossing—it corresponds to the vertex of the cone defined by the vanishing of the determinant of a symmetric matrix.

B. Frequency maps

In this section we will obtain some frequency maps for (21) using Laskar's method.[21] The basic idea is to approximately compute the frequencies for a particular initial condition by iterating for some fixed, finite time and extracting the frequencies in the resulting time series by computing their dominant spectral peaks. The frequency map can be computed by choosing a two-dimensional grid of initial conditions on a surface of fixed angles, by varying the actions. If each trajectory actually lies on an invariant torus, then this gives a numerical representation of the frequency map to the extent that a finite time series can be used to compute the frequencies. Of course there will be many chaotic trajectories, and for these the frequencies are not well-defined. Chaotic trajectories typically result in the frequencies not converging as the number of iterations is increased, and visually result in wild behavior of the frequency map.

Specifically, we iterate a grid of initial conditions using the quadratic approximation to the actions, i.e., the first two terms in (30). We arbitrarily fix the conjugate angles to 0 and take a grid of initial conditions in these (approximate) actions. For each point the corresponding coordinates (x,y) are calculated and then the orbit is iterated $2N+1$ times and the frequencies are calculated using a weighted Fourier transformation. As a weight function we use $1+\cos \pi t/(N+1)$, where $t \in [-N,N]$, the so-called Hann window. We take the sum over the four coordinates as the signal v_t from the orbit. The Fourier transform is defined by

$$\mathcal{F}(v;\Omega)=\frac{1}{2(N+1)}\sum_{t=-N}^{N} e^{2\pi i\Omega t}\left(1+\cos\frac{\pi t}{N+1}\right)v_t .$$

The maximum of the modulus of $\mathcal{F}(v;\Omega)$ as a function of Ω determines the first frequency, Ω_1. Note that we cannot use

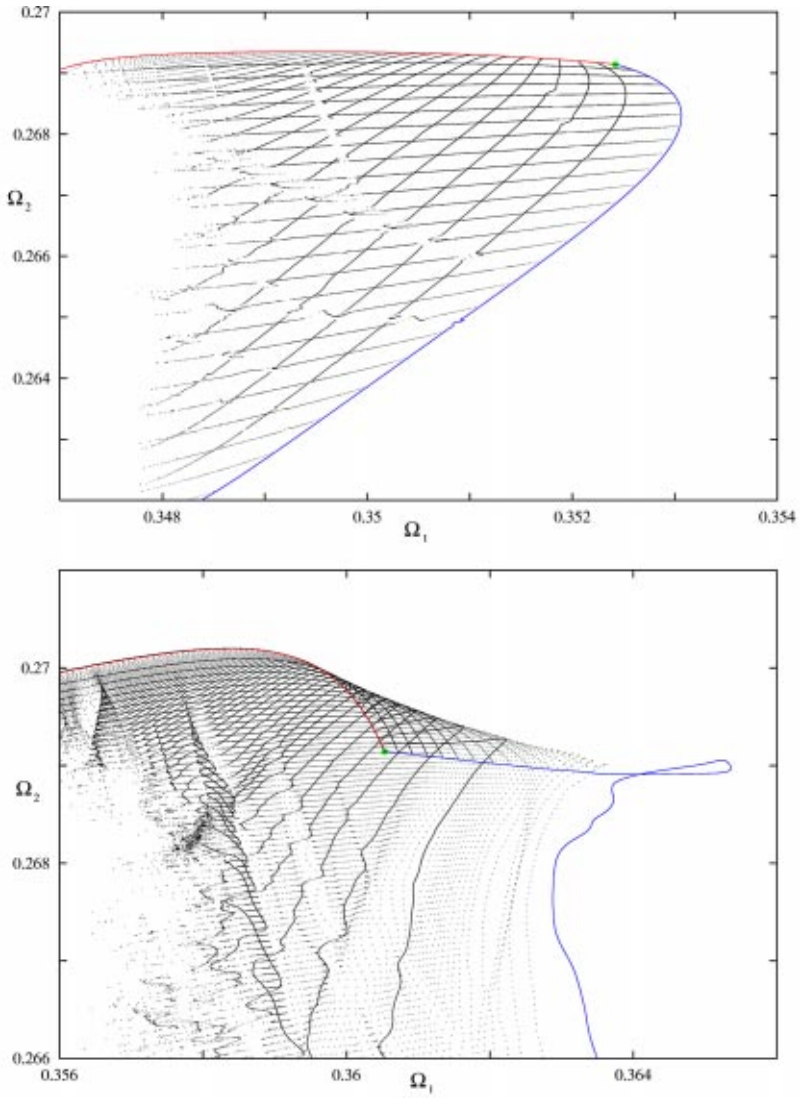

FIG. 12. (Color online) Frequency map near the twistless curve for $a_{ij}=0.1$ and $s_1s_2=1$. In the top panel $(R_1,R_2)=(0.80,0.56)$ so that $\omega=(0.3524,0.2691)$. The twist is $\tau_0=(1/100\pi)\,[(-6.82,1.13)^T,(1.13,-.514)^T]$, which is orientation preserving. In the bottom panel the first residue is now $R_1=0.82$ so that $\omega_1=0.3605$ and $\tau_0=(1/100\pi)\,[(-3.37,5.66)^T,(5.66,-0.469)^T]$ which is orientation reversing. In both figures the image of the J_1-axis intersects the Ω_2-axis.

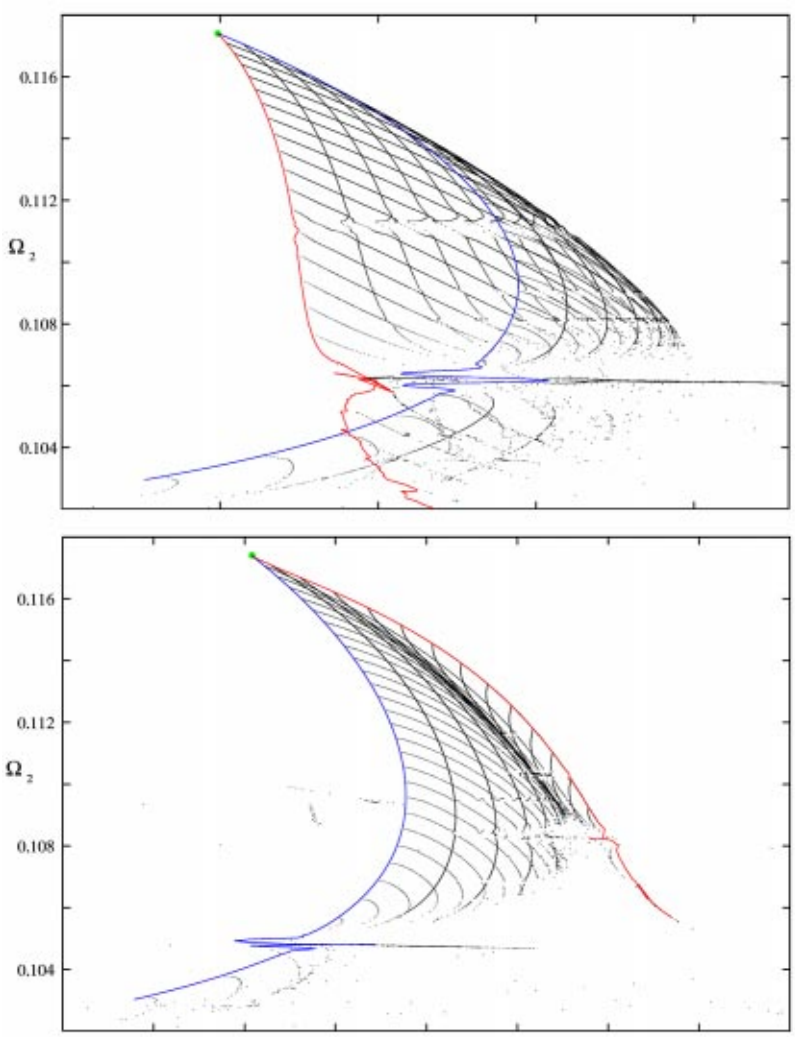

FIG. 13. (Color online) Frequency maps near a twistless curve for $a_{ij}=0.1$ and $s_1s_2=1$. In the top panel $(R_1,R_2)=(0.626,0.13)$ so that $\omega=(0.2905,0.1174)$. The twist matrix is $\tau_0=(1/100\pi)\,[(-0.929,-3.59)^T,(-3.59,-16.5)^T]$, so $\det\tau_0>0$. In the bottom panel the first residue is now $R_1=0.636$ so that $\omega_1=0.2938$, and $\tau_0=(1/100\pi)\,[(-0.769,-3.68)^T,(-3.68,-16.5)^T]$ which is now orientation reversing. Because the twist vectors are so nearly parallel we have applied a shear transformation to the figures to make the sector more visible, thus the units of the horizontal axis are arbitrary. In the top figure the image of the J_1-axis is on the left, while in the bottom figure it is on the right.

a FFT for this because we need very high accuracy in Ω_1. To find the second frequency, Ω_2, we remove the first frequency from the signal by forming $w_t=v_t-e^{-2\pi i\Omega_1 t}\mathcal{F}(v;\Omega_1)$. Then $\mathcal{F}(w;\Omega_2)$ is maximized. Frequencies are only defined up to unimodular transformations. When changing the parameters it is therefore possible that the largest peak appears at a different linear combination. To avoid such discontinuities in the frequency map we use a continuation method that tries to find local maxima near the previously found maxima.

In Fig. 12 parameters are chosen for the two panels on opposite sides of the $\det\tau_0=0$ curve. Here the top panel

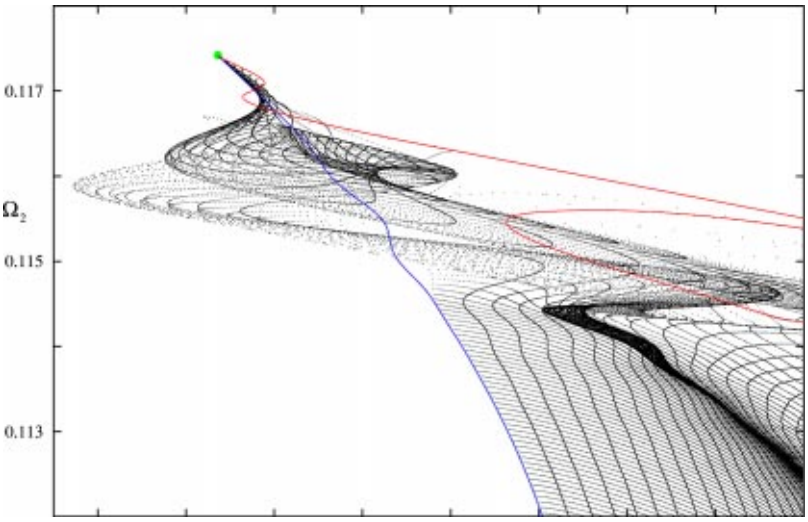

FIG. 14. (Color online) Frequency map for $a_{ij}=0.1$ and $s_1s_2=1$, and $(R_1,R_2)=(0.640,0.13)$ so that $\omega=(0.2952,0.1174)$. The twist matrix is $\tau_0=(1/100\pi)\,[(-0.698,-3.71)^T,(-3.71,-16.4)^T]$, so $\det\tau_0<0$. As in Fig. 13 the horizontal axis has been sheared and has arbitrary units. The image of the J_1-axis is eventually on the right.

shows that the twist columns are nearly antiparallel, and in the bottom panel, a fold singularity appears. Evidently, the slope of the singular curve is negative, so that the fold is created at the twistless bifurcation (recall Fig. 5). Note that there are resonances that cross the frequency map, as indicated by its oscillations. Also, chaotic orbits result in the breakup of the grid as the actions reach the outer boundary of the island.

In Fig. 13 parameters are chosen on opposite sides of the twistless bifurcation curve for the parallel case. A fold singularity is present in the top panel, and it disappears on the bottom. Evidently, the slope of the singular curve is negative, so that the fold is created at the twistless bifurcation (recall Fig. 2). However, in the bottom panel, there appears to be another singularity in the frequency map in the interior of the image of the positive quadrant, perhaps indicating that there is a nearby cusp in this case.

The behavior of this case becomes even more exotic upon a further increase of R_1, as shown in Fig. 14. For small values of the actions, the narrow wedge of the image of the positive quadrant is clearly visible, but for moderate actions, the image appears to undergo several spirals. The images of the J_1 and J_2 axes are particularly difficult to compute using the iterative method; in particular the frequency map is more sensitive to the number of iterates used in this case than when both actions are nonzero. This is reflected in the rapid change in the frequencies in the figure when J_2 in particular is increased from zero.

VI. CONCLUSIONS

We have shown that twistless bifurcations occur in one-parameter families of symplectic maps when the elliptic fixed point is near a tripling resonance, where $\omega_i = \frac{1}{3}$. The simplest such bifurcation corresponds to the fold singularity; it leads to the reversal of the orientation of the frequency map and a domain on which the map is two-to-one.

A fold singularity at an elliptic fixed point is manifested in one of several ways depending upon whether the columns of the twist matrix are parallel or antiparallel and whether the slope of the singular curve is positive or negative. We have calculated the twist for a quadratic example and shown that it predicts where this phenomenon is observed in computations of the frequency map from iterative data. Though our twist formulas apply for the case of mixed Krein signatures, we have not investigated the effect of these on the dynamics.

Since the two-dimensional twistless bifurcation creates a twistless invariant circle and reconnection bifurcations, we can expect that similar phenomena occur in the four-dimensional case. We are currently investigating these.

It would also be interesting to investigate the occurrence of cusp singularities, which would require knowing the twist through first order in the action variables. Since the local frequency map in the neighborhood of a cusp is three-to-one, it should be possible for reconnection bifurcations to occur between three resonances with the same frequency vector. The dynamical effect of this on neighboring invariant tori should be as dramatic as the meandering invariant curves that occur near a reconnection in two dimensions.

ACKNOWLEDGMENTS

H.R.D. was supported in part by the EPSRC Grant No. GR/R44911/01, DFG Grant No. Du 302/2, and the European Commission Grant No. HPRN-CT-2000-00113 (''MASIE''). J.D.M. was supported in part by NSF Grant No. DMS-0202032 and the NSF-VIGRE Grant No. DMS-9810751.

APPENDIX: MOSER'S NORMAL FORM FOR QUADRATIC MAPS

Moser[29,33] showed that any four-dimensional, quadratic, symplectic map can be transformed by an affine coordinate change into a normal form with six parameters and two indices. This map is generated by the Lagrangian

$$\tilde{L}(x,x') = -x'^{T}Cx - U(x),$$

where $U(x) = a_1x_1 + a_2x_2 + \frac{1}{2}bx_1^2 + x_1(\epsilon' x_1^2 + x_2^2)$, and C is a 2×2 matrix such that $\det(C) = \epsilon$. The six parameters are the three elements of C and a_1, a_2, b; the indices are $\epsilon = \pm 1$, and $\epsilon' = 0, \pm 1$. Geometrically, ϵ corresponds to the product of the Krein signatures, and ϵ' to the discriminant of the cubic terms.

When the matrix C is symmetric, Moser's normal form can be transformed to the standard form (16) with the symplectic coordinate change $(x,y) \to (\hat{x},\hat{y})$ generated by

$$F(x,\hat{x}) = x^{T}C\hat{x} + \tfrac{1}{2}\hat{x}^{T}C\hat{x} + U(\hat{x}).$$

This gives a map generated by a Lagrangian of the form (16), where the kinetic energy is $K(v) = v^{t}Cv/2$ and potential $V(x) = x^{T}Cx + U(x)$. If, in addition, the map has a fixed point, we can shift coordinates so that the fixed point is at the origin. In this case, the linear terms in V become zero.

It is interesting that ϵ', the discriminant of the cubic part of U, is also the discriminant of V. The other sign, corresponding to the determinant of C, is equivalent to the product of the signatures, $\epsilon = s_1 s_2$.

Finally, if there is a linear transformation that simultaneously diagonalizes the kinetic energy and the quadratic part of V, then this transformation can be used to put the map in our form (21). A sufficient condition for simultaneous diagonalization is that K is definite, so that $\epsilon = 1$.

If the Krein signatures are not equal, the simultaneous diagonalization is not always possible. It still can be done, however, if one of the matrices is ''diagonally dominant.'' If not, we need a general symplectic transformation instead of just a point transformation to diagonalize the quadratic terms. This more general transformation will mix coordinates and momenta, and therefore will destroy the simple structure ''kinetic plus potential'' of the generating function.

We conclude that our map is equivalent to the general case when there is a strongly-stable fixed point, and when C is symmetric and the simultaneous diagonalization can be done. This certainly includes the case of a ''natural'' map.

[1] V. I. Arnold, *Mathematical Methods of Classical Mechanics* (Springer, New York, 1978).
[2] K. R. Meyer and G. R. Hall, *Introduction to the Theory of Hamiltonian Systems*, Vol. 90 of *Applied Mathematical Sciences* (Springer-Verlag, New York, 1992).

[3] R. Moeckel, ''Generic bifurcations of the twist coefficient,'' Ergodic Theor. Dyn. Syst. **10**(1), 185–195 (1990).
[4] H. R. Dullin, J. D. Meiss, and D. Sterling, ''Generic twistless bifurcations,'' Nonlinearity **13**, 203–224 (1999).
[5] J. P. van der Weele, T. P. Valkering, H. W. Capel, and T. Post, ''The birth of twin Poincaré–Birkhoff chains near 1:3 resonance,'' Physica A **153**, 283–294 (1988).
[6] J. P. van der Weele and T. P. Valkering, ''The birth process of periodic-orbits in non-twist maps,'' Physica A **169**, 42–72 (1990).
[7] T. P. Valkering and S. A. Vangils, ''Bifurcation of periodic-orbits near a frequency maximum in near-integrable driven oscillators with friction,'' Z. Angew. Math. Phys. **44**(1), 103–130 (1993).
[8] C. Simó, ''Stability of degenerate fixed points of analytic area-preserving mappings, bifurcation, ergodic theory and applications,'' Astérisque **98**, 184–194 (1982).
[9] H. E. Cabral and K. R. Meyer, ''Stability of equilibria and fixed points of conservative systems,'' Nonlinearity **12**, 1351–1362 (1999).
[10] J. E. Howard and S. M. Hohs, ''Stochasticity and reconnection in Hamiltonian systems,'' Phys. Rev. A **29**, 418–421 (1984).
[11] J. E. Howard and J. Humpherys, ''Nonmonotonic twist maps,'' Physica D **80**, 256–276 (1995).
[12] A. D. Morozov, ''Degenerate resonances in Hamiltonian systems with 3/2 degrees-of-freedom,'' Chaos **12**, 539–548 (2002).
[13] C. Simó, ''Invariant curves of analytic perturbed nontwist area-preserving maps,'' Regular Chaotic Motion **3**(3), 180–195 (1998).
[14] D. del Castillo-Negrete, J. M. Greene, and P. J. Morrison, ''Area-preserving nontwist maps: Periodic orbits and transition to chaos,'' Physica D **91**, 1–23 (1996).
[15] D. del Castillo-Negrete, J. M. Greene, and P. J. Morrison, ''Renormalization and transition to chaos in area-preserving nontwist maps,'' Physica D **100**, 311–329 (1997).
[16] A. Delshams and R. de la Llave, ''KAM theory and a partial justification of Green's criterion for nontwist maps,'' SIAM (Soc. Ind. Appl. Math.) J. Math. Anal. **31**, 1235–1269 (2000).
[17] A. D. Morozov and S. A. Boykoya, ''On the investigation of degenerate resonances,'' J. Regular Chaotic Dyn. **4**(1), 70–82 (1999).
[18] R. Thom, ''Singularities of differentiable mappings. I,'' in *Proceedings of Liverpool Singularities. Symposium 1-2*, Vol. 192, edited by C. T. C. Wall (Springer-Verlag, Berlin, 1971).
[19] V. I. Arnold, ''Critical points of functions and the classification of caustics,'' Usp. Mat. Nauk **29**(3), 243–244 (1974).
[20] J. Laskar, ''Frequency analysis for multi-dimensional systems. Global dynamics and diffusion,'' Physica D **67**, 257–283 (1993).
[21] J. Laskar, ''Introduction to frequency map analysis,'' in *Hamiltonian Systems with Three or More Degrees-of-freedom (S'Agaro, 1995)*, Vol. 533 of *NATO Adv. Sci. Inst. Ser. C Math. Phys. Sci.*, edited by C. Simó (Kluwer, Dordrecht, 1999), pp. 134–150.
[22] J. D. Meiss, ''Average exit time for volume preserving maps,'' Chaos **7**, 139–147 (1997).
[23] V. I. Arnold, S. M. Gusein-Zade, and A. N. Varchenko, *Singularities of Differentiable Maps, Volume I*, Vol. 82 of *Monographs in Mathematics* (Birkhauser, Boston, 1985).
[24] A. Weinstein, *Lectures on Symplectic Manifolds*, Vol. 29 of *Regional Conference Series in Mathematics* (AMS, Providence, 1977).
[25] H. R. Dullin, A. Ivanov, and J. D. Meiss, ''The standard cusp map,'' Technical report, Univ. of Colorado, in preparation.
[26] J. D. Meiss, ''Symplectic maps, variational principles, and transport,'' Rev. Mod. Phys. **64**, 795–848 (1992).
[27] G. H. Hardy and E. M. Wright, *An Introduction to the Theory of Numbers* (Oxford University Press, Oxford, 1979), Theorem 25.
[28] B. V. Chirikov, ''A universal instability of many-dimensional oscillator systems,'' Phys. Rep. **52**, 265–379 (1979).
[29] J. K. Moser, ''On quadratic symplectic mappings,'' Math. Z. **216**, 417–430 (1994).
[30] M. Hénon, ''Numerical study of quadratic area-preserving mappings,'' Q. Appl. Math. **27**, 291–312 (1969).
[31] J. E. Howard and H. R. Dullin, ''Linear stability of natural symplectic maps,'' Phys. Lett. A **246**, 273–283 (1998).
[32] C. F. F. K. Karney, A. B. Rechester, and R. B. White, ''Effect of noise on the standard mapping,'' Physica D **4**, 425–438 (1982).
[33] K. E. Lenz, H. E. Lomelí, and J. D. Meiss, ''Quadratic volume preserving maps: An extension of a result of Moser,'' Regular Chaotic Motion **3**, 122–130 (1999).